Hindawi
International Journal of Antennas and Propagation
Volume 2023, Article ID 7157515, 12 pages
https://doi.org/10.1155/2023/7157515

Research Article

Design of an Enhanced Isolation 8-Unit MIMO Antenna for Smartphones Operating in 5G nR and LTE 42 Bands

Zhiwei Song,[1] **Hongxiang Miao**,[1] **Xiaoming Xu**,[1] **and Lu Wang**[2]

[1]*School of Electrical Engineering, Xinjiang University, Huarui Street 777#, Shuimogou District, Wulumuqi, Xinjiang, China*
[2]*The 58th Research Institute of China Electronics Technology Group Corporation, Wuxi, China*

Correspondence should be addressed to Zhiwei Song; suzawer@163.com

Received 29 April 2023; Revised 9 June 2023; Accepted 19 June 2023; Published 30 June 2023

Academic Editor: Trushit Upadhyaya

A miniaturized enhanced isolation 8-unit MIMO antenna for smartphones is proposed in this paper. The units are planar inverted-F antennas with the same structure, and we use the slotting method and shorted probe to miniaturize them. The size of every unit is $14 \times 6\,\text{mm}^2$ ($0.149 \times 0.064\lambda^2$). We insert an L-shaped decoupling element into the middle of adjacent radiating elements and connect the decoupling element to the GND. Note that the decoupling elements are on the outer side of the substrate, and the radiating elements are on the inner side of the substrate. Finally, a prototype is fabricated and measured. The measured results show that the bandwidth of the MIMO antenna is from 3.0 GHz to 5.3 GHz (55.4%), which fully supports the *n*77, *n*78, and *n*79 in the 5G nR frequency band and the 4G LTE 42 frequency band (S_{11} less than −6 dB). The measured isolation of the MIMO antenna is greater than 25 dB by using the decoupling method in this paper. The envelope correlation coefficient of the proposed MIMO antenna is less than 0.08, its radiation efficiency is greater than 50%, and its gain is between 4.2 and 5.3 dBi in the whole operating frequency band.

1. Introduction

Due to the use of higher communication frequency bands in the fifth-generation mobile communication (5G), it can provide higher capacity and efficiency than its predecessor [1–4]. In particular, 5G New Radio (5G nR) is an offshoot of the 5G standard that employs advanced technologies such as massive multiple-input multiple-output (MIMO) antennas to achieve high data rates and spectral efficiency. However, MIMO antennas also face many challenges in practical applications, such as poor isolation between antenna units [4–6]. Since the available space in mobile devices is limited, how to improve the isolation between MIMO antenna units is currently a research hotspot.

To address these challenges, researchers have proposed various decoupling methods to improve the isolation between antenna elements [7–22]. These methods include defect grounding structures [7–10], decoupling networks [11–17], and orthogonal polarization [18, 19]. The simplest and most direct method is to change the distance between the antennas to reduce the mutual influence between them. However, due to the limited space of the equipment, increasing the distance between the antennas will sacrifice the number of antenna elements, resulting in channel attenuation. In addition, for example, the defect grounding structure mainly changes the electric field distribution on the ground surface by slotting in the GND, to reduce the coupling effect. In [10], a planar inverted-F antenna (PIFA) antenna array is loaded with a short-circuit unit, an L-shaped structure, and a C-shaped branch, which can cover the 3.3–6.0 GHz frequency band.

Recently, a self-isolation method was proposed in [17], and the radiation unit is also used as a decoupling unit. This method can greatly improve the isolation between antenna units, but the antenna only covers the 3.4–3.6 frequency band, which cannot meet the requirements of 5G current needs.

In [18], the authors propose an 8-cell slit antenna operating in the 5G nR band, covering 3.3–5.0 GHz; the isolation is about 12 dB.

There is also an orthogonal polarization method. By changing the polarization direction of the antenna, the adjacent polarization directions are vertically combined, and no additional space is required. In [19], the orthogonal polarization method is used to improve the isolation, but it cannot cover a wide frequency band and can only be applied to a single frequency band.

In conclusion, these methods have their advantages and limitations, which limit their use in 5G nR applications.

In this paper, a wideband miniaturized enhanced isolation 8-unit MIMO antenna is proposed. The slotting method and shorting post are used to gain the miniaturization of the antenna unit. The geometry of the unit is a slotted planar inverted-F antenna (SPIFA), and the size of every unit is $14 \times 6\,\text{mm}^2$. To enhance the isolation, we insert an L-shaped decoupling element into the middle of adjacent radiating elements and connect the decoupling element to the GND. Note that the decoupling elements are on the outer side of the substrate, and the radiating elements are on the inner side of the substrate. The isolation is greatly improved by using this method, and the measured isolation is greater than 25 dB in the whole operating frequency band. The measured bandwidth of the MIMO antenna is from 3.0 GHz to 5.3 GHz, and the fractional bandwidth ($S_{11} < -6$ dB) reaches 55.4%, which fully covers the requirements of the 5G nR network ($n77$/$n78$/$n79$ and LTE 42). The envelope correlation coefficient (ECC) is less than 0.08 in the 5G nR frequency band. The diversity performance of the proposed MIMO antenna is excellent, the radiation efficiency is greater than 50%, and its gain is between 4.2 and 5.3 dBi in the whole operating frequency band.

2. Topology and Design Strategy

The geometry of the designed MIMO antenna and its units is shown in Figure 1. The overall size of the MIMO antenna is $150.0 \times 70.0 \times 7.0\,\text{mm}^3$. The MIMO antenna is composed of a horizontal substrate, two vertical substrates, eight SPIAs, eight shorted probes, eight 50 Ω impedance matching microstrip feedlines, six L-shaped decoupling units, and eight SMAs. The three substrates are made of printed circuit boards (FR4) which have a relative dielectric constant of 4.4 and a loss angle tangent of 0.02. The horizontal substrate thickness is 1.0 mm, and the vertical substrate thickness is 0.8 mm. The antenna units are placed on the inner surfaces of the two vertical substrates, and the L-shaped decoupling units are placed on the outer surface of the two vertical dielectric substrates.

2.1. The Geometry of the Antenna. The SPIFA design is a popular choice for wideband communication systems due to its low profile and ease of integration with other components. In this case, the antenna is designed to meet the coverage requirements of 5G nR broadband, which is characterized by a high data rate and a low latency. The miniaturization is gained by using the slotting method in the radiation patch. The initial shape of the radiation patch is rectangular, with a size of $14.0 \times 6.0\,\text{mm}^2$ ($0.149 \times 0.064\lambda^2$), where λ corresponds to the wavelength of the minimum working frequency in free space (3.1 GHz). The antenna unit consists of four parts: a radiation patch, a short-circuit branch, a 50 Ω impedance matching microstrip line, and a feed port. And the radiation unit is mainly composed of three parts, namely, L1, L2, and L3, respectively, as shown in Figure 1. The first (L1) part and the second part (L2) of the radiation patch are L-shaped structures, and the third part (L3) is an inverted U-shaped structure. The short arm of L1 is connected to the short-circuit branch and then connected to the GND by the shorted probe. The short rectangular tail of L3 links has a 50 Ω impedance matching microstrip line.

The coupling unit, which is an L-shaped structure with dimensions of $12 \times 7\,\text{mm}^2$ as shown in Figure 1, is added to the design to improve the isolation. Isolation refers to the ability of the antenna to prevent signals from interfering with each other. The addition of the coupling unit increases the isolation by 8 dB under simulation and 15 dB in actual measurement, which is a significant improvement. Overall, this broadband SPIFA design is a promising solution for meeting the coverage requirements of 5G nR broadband, and the addition of the decoupling unit further improves its performance.

2.2. Evolution of the Design. The design of the proposed array unit involves three steps, as shown in Figure 2.

Step 1: only a rectangular radiation patch without slots, as shown in Figure 2(a)

Step 2: the radiation patch is divided into three parts, as shown in Figure 2(b)

Step 3: the proposed geometry, as shown in Figure 2(c)

The S_{11} of each step in the simulation is depicted in Figure 3. In step 1, the center frequency is 3.4 GHz. In step 2, end-opening slots are added to the radiation patch, and the patch is divided into three parts; therefore, the effective radiation patch area is reduced, and the center frequency of the antenna unit is 4.78 GHz. In step 3, we cut a U-shaped slot on the right bottom corner of the patch. By performing slot processing and changing the current flow direction, the final design is obtained. The antenna bandwidth ranges from 3.1 GHz to 5.5 GHz with two operating frequency points of 3.2 GHz and 4.8 GHz, covering 5G nR ($n77$/$n78$/$n79$) and 4G LTE 42 bands. To further understand the radiation characteristics of the antenna, the analog distribution of the current of the antenna unit at various operating frequencies is shown in Figure 4. At 3.2 GHz, the electric currents are mostly distributed in two L-shaped regions with long current paths, resulting in a correspondingly lower operating frequency. At 4.8 GHz, the electric currents are dominated in the U-shaped region with shorter current paths, resulting in a correspondingly higher working frequency.

2.3. Key Parameters Simulation Analysis. During the antenna design process, some key parameter changes have a remarkable effect on the antenna's radiation characteristics. In the following text, we have selected two of them for

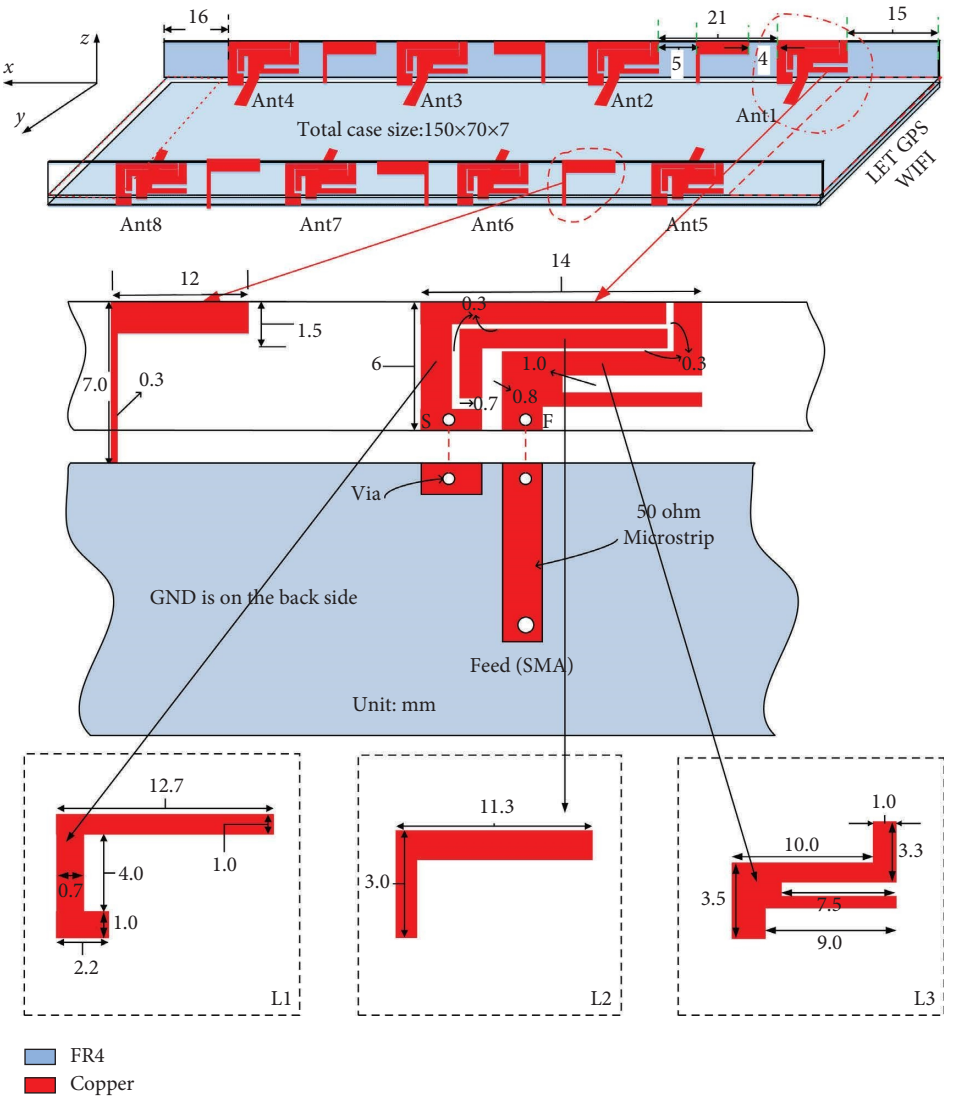

Figure 1: Geometry and dimensions of array antenna elements.

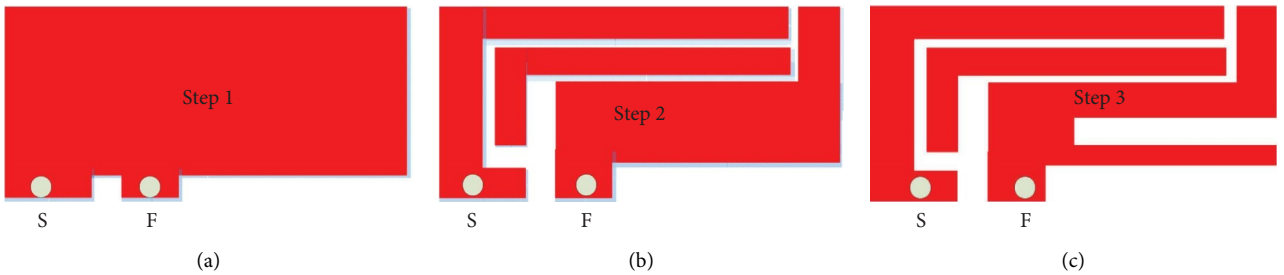

Figure 2: The evolution of radiation patch structures. (a) Step 1, (b) step 2, and (c) step 3.

detailed discussion. $S1$ is the length of the bigger L-shaped radiation patch, as shown in Figure 5. The simulation S_{11} at different sizes is illustrated in Figure 5, too. The two working frequency points change a little, but the impedance matching changes greatly when $S1$ changes. So, we can adjust the impedance matching by changing this parameter.

The simulated S_{11} when the depth ($S2$) of the U-shaped slot changes is shown in Figure 6. The changes in $S2$ have little impact on low-frequency operating frequency points but have a significant impact on the bandwidth and the high-frequency operating frequency points. Therefore, we can adjust the high-frequency operating frequency points and

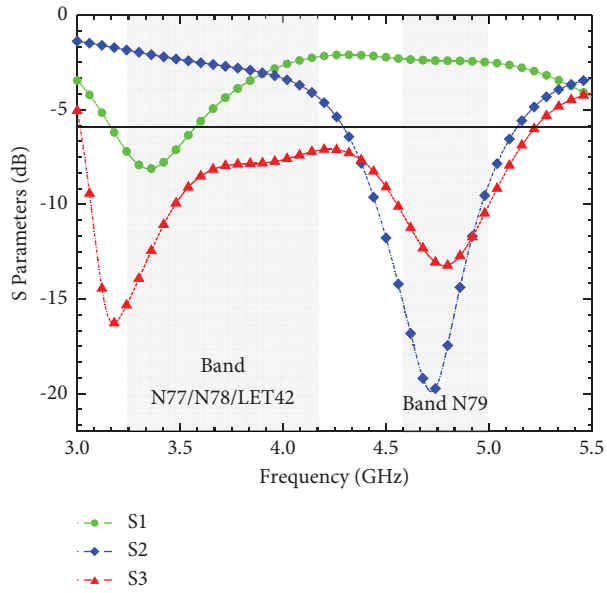

Figure 3: The simulation results of S_{11} of three steps.

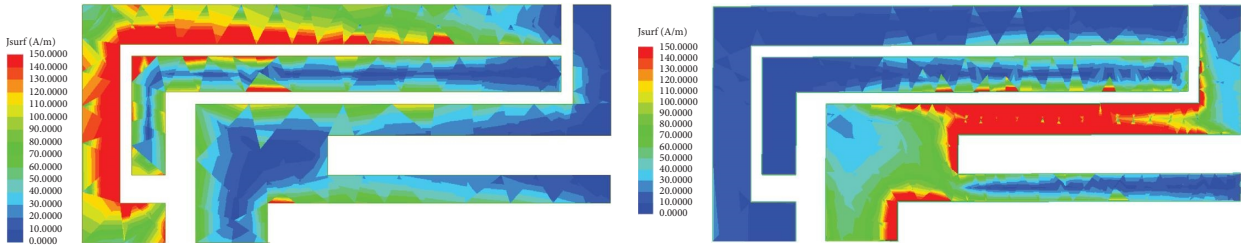

Figure 4: Current distribution on the antenna radiation patch unit. (a) 3.2 GHz. (b) 4.8 GHz.

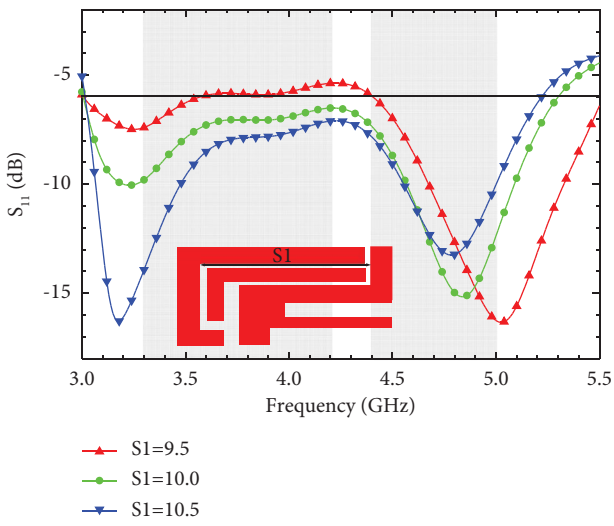

Figure 5: The simulation results of S_{11} when $S1$ has different sizes.

the bandwidth by changing this parameter. Many other parameters can affect the radiation characteristics of the MIMO antenna, but we do not show them for brevity.

2.4. Decoupling Unit Simulation Analysis. The very close proximity of the MIMO antenna units due to the mobile phone's limited space inevitably has a detrimental effect on the isolation between adjacent antenna units. To solve the above problem, an L-shaped decoupling unit is introduced between the neighboring antenna units, depicted in Figure 1. The decoupling units are placed on the outer surface of the two perpendicular dielectric substrates, and the antenna units are on the inner surface of the two perpendicular dielectric substrates. Furthermore, L-shaped decoupling units are connected to the GND. The simulated electric field distribution with and without L-shaped decoupling units at different phases is depicted in Figure 7. Therefore, it is clear that the coupling electric field between adjacent antenna units is significantly reduced after the decoupling structure is added, which helps to increase the isolation between the radial units.

To visualize the antenna isolation before and after the decoupling structure is added, the simulated return loss characteristics are displayed in Figure 8. From Figure 8, the isolation between adjacent antenna units increases by 8.9 dB with a minimum isolation of more than 20 dB after the addition of the decoupling structure.

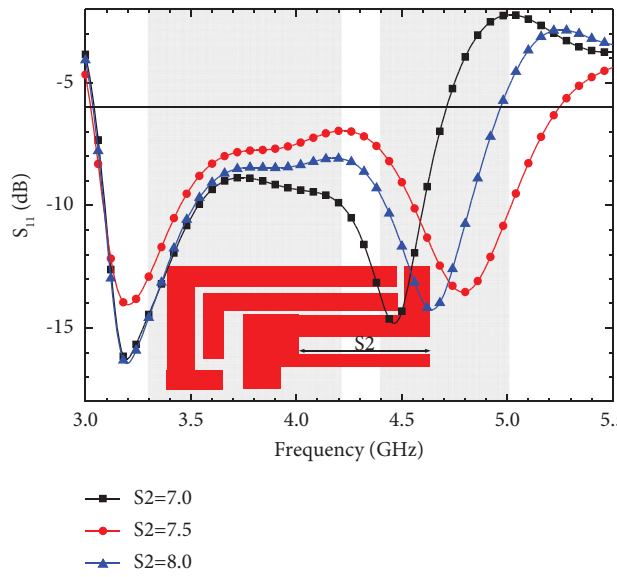

Figure 6: The simulation results of S_{11} when $S2$ has different sizes.

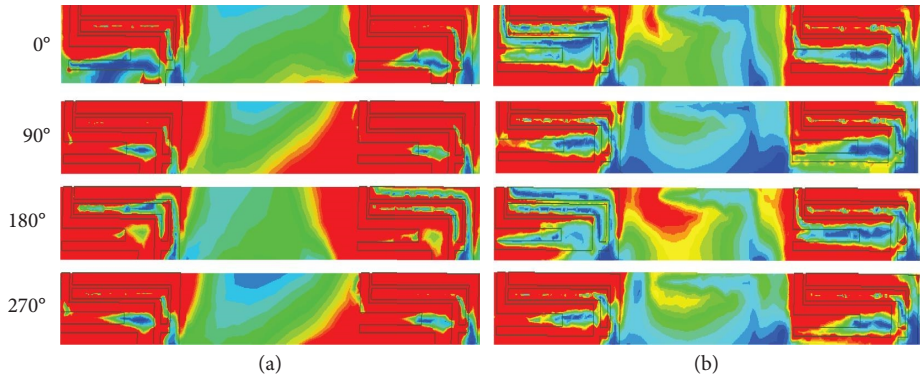

Figure 7: Electric field distributions between adjacent units at 3.3 GHz: (a) antenna without an L-shaped decoupling unit and (b) antenna with an L-shaped decoupling unit.

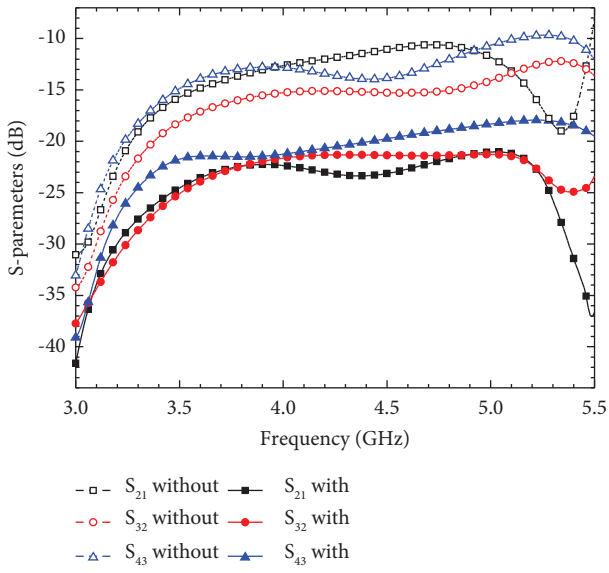

Figure 8: The simulated isolation when the MIMO antenna is without/with L-shaped decoupling units.

Simulations S_{11}–S_{44} with and without decoupling units are presented in Figure 9. The results show that without the L-shaped coupling unit, the operating band almost covers 3.0–5.3 GHz, with a reflection factor of slightly less than 10 dB at 3.1 GHz. Although the introduction of the L-shaped coupling unit improves the isolation between antennas by about 8.9 dB, it hurts the antenna performance. However, the degree of deterioration is tolerable, and the antenna's working frequency band can still cover 3.0–5.3 GHz, thereby ensuring the normal operation of the antenna in the 5G nR and LTE 42 frequency bands.

3. Measurement and Analysis

We have made physical objects and carried out measurements, the physical photographs of which are shown in Figure 10. The S-parameters were tested using a PNA-X vector network analyzer, and the far-field radiation characteristics were measured in an anechoic chamber. A screenshot of the experimental scenario is depicted in Figure 11. After the analysis and discussion of the test results, the simulations are carried out.

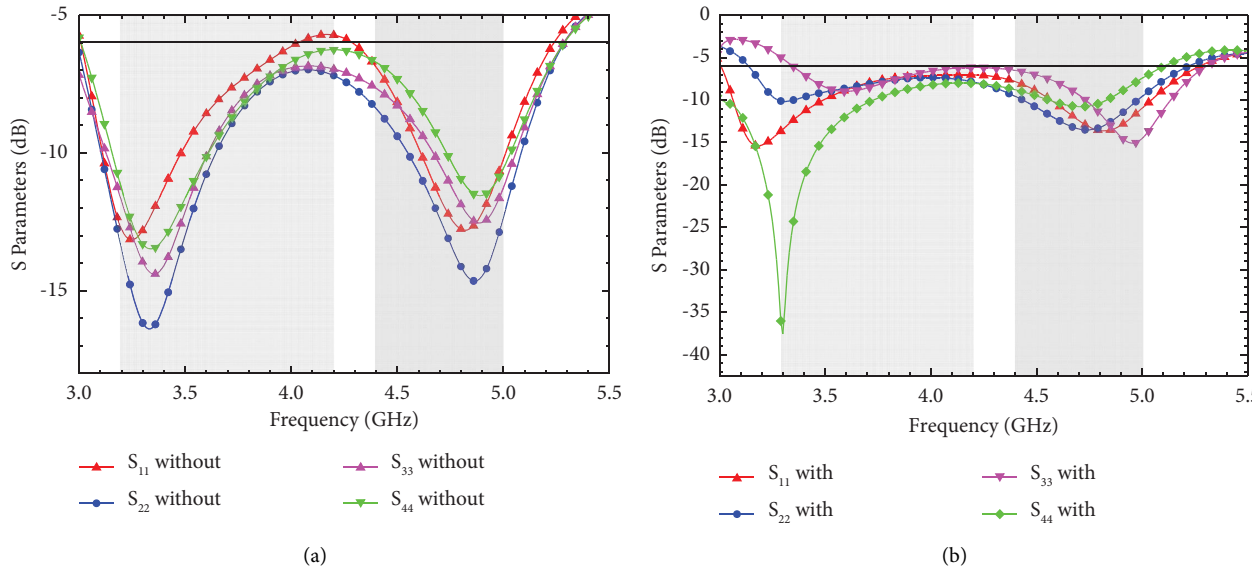

Figure 9: The simulated *S*-parameters when the MIMO antenna is (a) without L-shaped decoupling units and (b) with L-shaped decoupling units.

Figure 10: Photos of the manufactured MIMO antenna: (a) front view, (b) back view, and (c) 3D view.

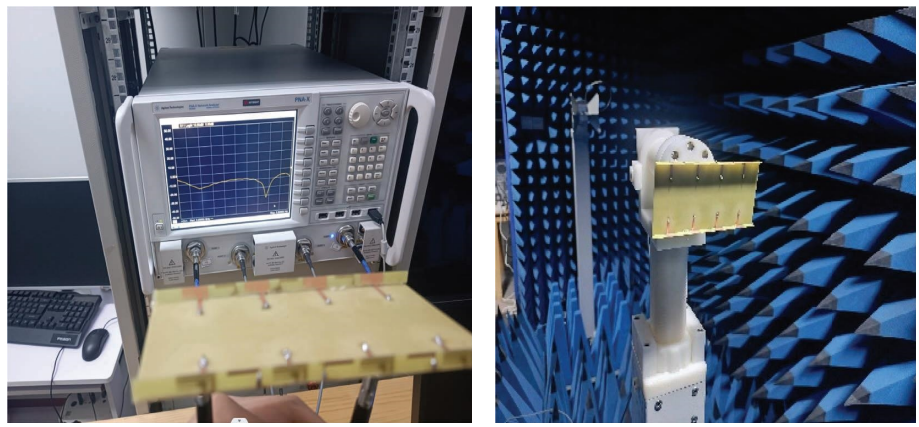

Figure 11: Pictures of the antenna when it is measured.

3.1. The Analysis of the Measurement Results. Figure 1 shows the layout of the 8-unit MIMO antenna (Ant. 1-Ant. 8) and the parametric structure of the decoupling structure in detail. Ant. 1–Ant. 4 and Ant. 5–Ant. 8 are placed in the device frame. Ant. 1–Ant. 4 and Ant. 5–Ant. 8 are in a mirror-image relationship. To discuss the results, only one of them is selected for presentation. The total length of Ant. 1–1Ant. 4 is 119.0 mm, the length of the unit is 14.0 mm, the gap between adjacent units is 21.0 mm, and the decoupling unit is placed in the middle of the gap (its length is 12.0 mm).

The measured return loss and isolation of the MIMO antenna are depicted in Figures 12 and 13, respectively. When comparing the simulation with the actual measurement results, we first compared the reflection coefficients shown in Figures 9(b) and 12 (S_{11}, S_{22}, S_{33}, and S_{44}) and then the isolation parameters (S_{21}, S_{32}, and S_{43}) shown in

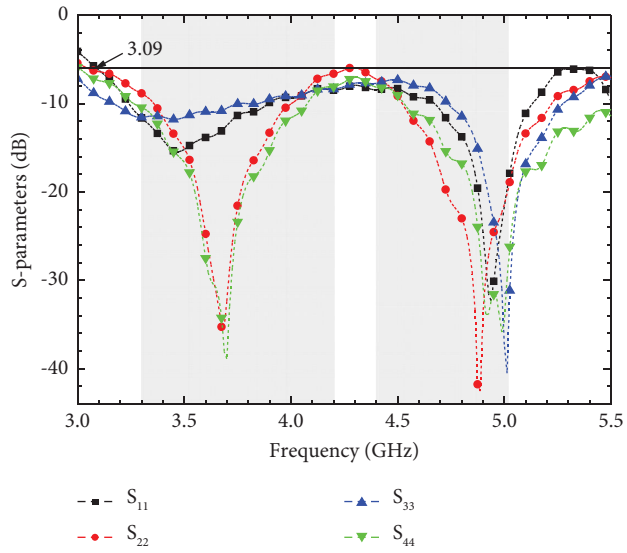

Figure 12: The measured *S*-parameters of the designed MIMO antenna.

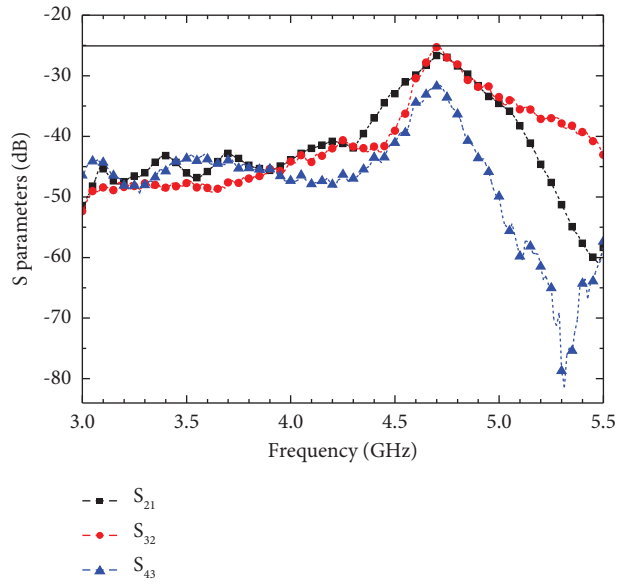

Figure 13: The measured isolation of the designed MIMO antenna.

Figures 8 and 13. From the comparison results, the simulated and measured results have some errors, but the actual measurement results are better to a certain extent, especially in terms of isolation, where the simulation results showed isolation up to 19.0 dB while the measured result reached 25.0 dB, which is better than expected.

In terms of impedance bandwidth and coupling, the simulation results show an impedance bandwidth of 55.4% (3.0–5.3 GHz) and 19.0 dB isolation between antenna elements, as displayed in Figures 8 and 9(b). The test results illustrate a good impedance bandwidth of 56.1% (3.09–5.5 GHz) and an excellent isolation of 25 dB, particularly in terms of coupling. In summary, the designed 8-unit MIMO antenna has a good bandwidth, covering the entire 5G nR band (*n*77/*n*78/*n*79) and the LTE 42 band with excellent isolation.

3.2. Performance and Radiation Direction. The ECC indicates the signal correlation between two adjacent antennas, and the ECC directly affects the MIMO antenna channel capacity. The ECC is shown in Figure 14. It can be seen that the ECC factor is less than 0.08 in the 5G nR and LTE 42 bands, and the channel capacity is between *X*-*X*1 bps/Hz, which is slightly less than the upper limit of 46 bps/Hz for an 8-unit MIMO antenna. The mean effective gain (MEG) ratio is a significant characteristic to elevate the MIMO antenna performance, which is calculated by using the ratio of the mean receive power and the mean incident power. And the calculated MEGs of Ant. 1–4 are shown in Figure 15. The ratios of the MEG should satisfy the following criteria to guarantee good channel characteristics[23]:

$$\frac{\left|\mathrm{MEG}_i\right|}{\left|\mathrm{MEG}_j\right|} \cong 1, \tag{1}$$

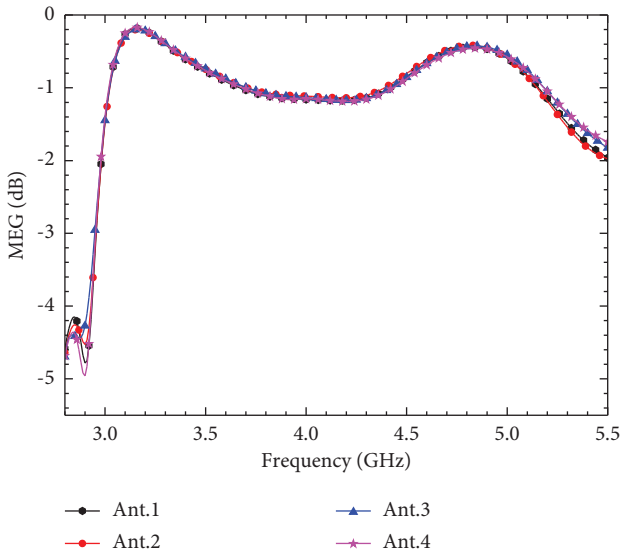

Figure 14: The calculated MEGs of Ant. 1, Ant. 2, Ant. 3, and Ant. 4.

where i and j are integers belonging to 1 to 4, and i is not equal to j.

The MEGs of the four antenna elements of the MIMO antenna belonging to one side are nearly identical over the whole operating frequency band, which suggests a good channel performance.

The measured radiation efficiencies are shown in Figure 16. The overall efficiency of the antenna fluctuates between 29% and 98%, with an overall efficiency greater than 50% in the 5G nR band, indicating good performance. To consider the impact of electromagnetic radiation on the human body in practical applications, a human model was added as a reference object, and the male head was used as

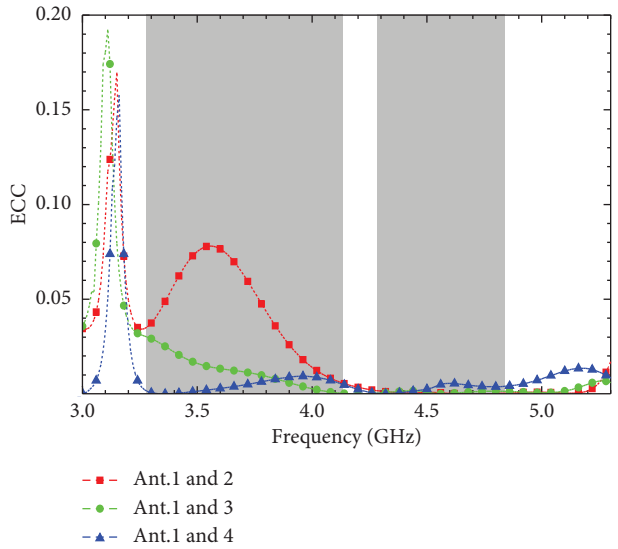

Figure 15: The ECC of the designed MIMO antenna.

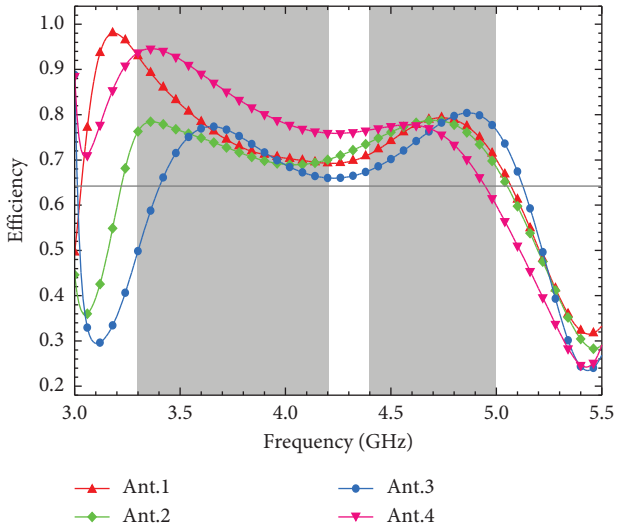

Figure 16: The designed MIMO antenna's measured radiation efficiency.

the observation object for simulation tests in HFSS, as shown in Figure 17. The test result's SAR maximum value was only 0.054 W/kg, which fully meets the standard of 1.6 W/kg of the IEEE International Conference, ensuring safety in practical applications.

Figure 18 shows the measured and simulated radiation patterns of Ant. 1–Ant. 4 at different frequencies. It can be seen that the error between the simulated and measured results is small. At 3.3 GHz, the radiation direction of Ant. 1 and Ant. 4 is mainly in $-Y$. Under the influence of the coupling units on both sides, the radiation direction of Ant. 2 and Ant. 3 changes, the radiation in the Y direction is weakened, and the radiation in the X direction is enhanced; therefore, the influence between the antennas is weakened, leading to a reduction in coupling.

As a result, the influence between the antennas is weakened, and the coupling is reduced. At 4.8 GHz, it can be seen that the direction of radiation in the E- and H-planes is essentially the same as that at 3.3 GHz. On the device, the

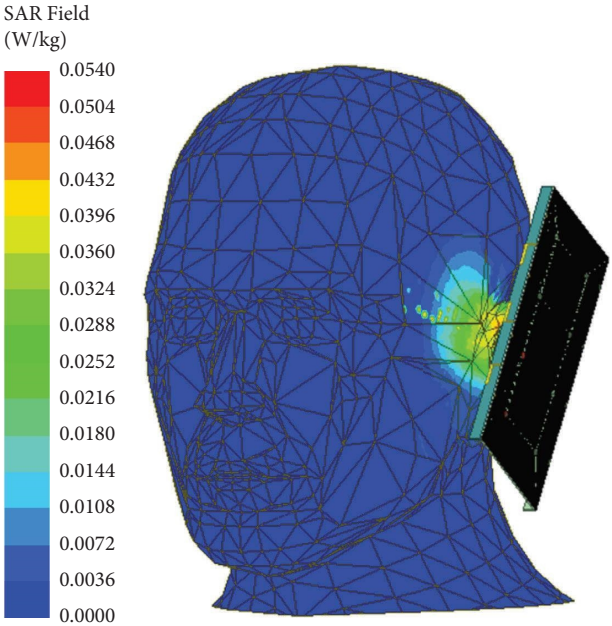

Figure 17: The simulated SAR when a male head model is inserted.

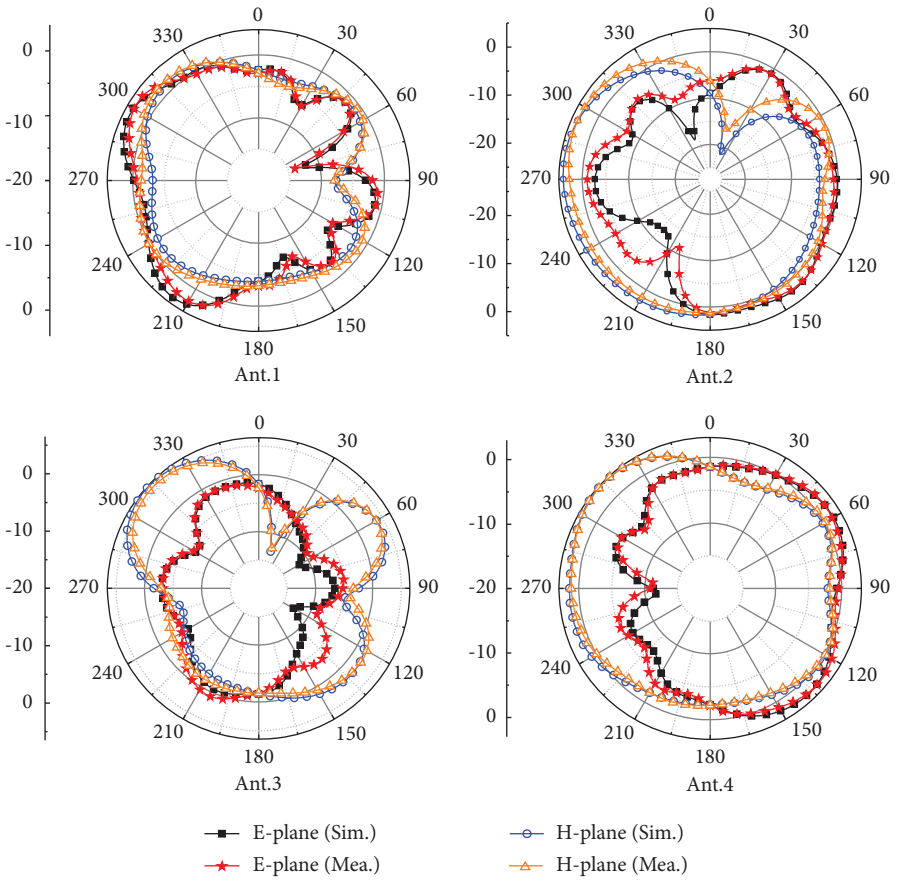

(a)

Figure 18: Continued.

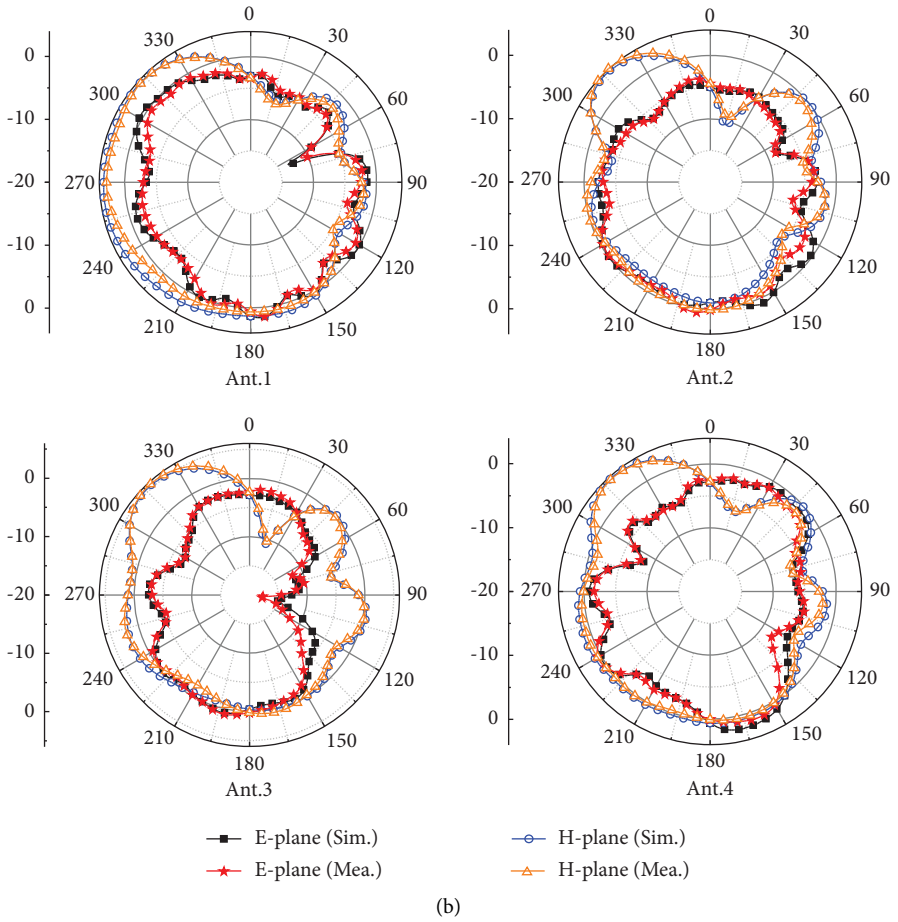

(b)

Figure 18: The measured and simulated radiation patterns of ant. 1 to ant. 4. (a) 3.3 GHz. (b) 4.8 GHz.

Table 1: Comparison with previous published literature.

Ref	AAE size ($L \times H$)	BW (GHz)	Isolation (dB)	ECC	TE
[8]	16.0 × 6.0	3.42–3.69	24.0	0.01	49.0%
[15]	18.6 × 7.0	3.3–4.2 4.8–5.0	12.5	0.12	53.0%
[20]	40.0 × 3.0	3.3–5.0	12.0	0.11	31.0%
[22]	30.0 × 7.0	3.3–7.5	10.0	0.05	40.0%
[24]	15.0 × 7.0	3.4–3.6 4.8–5.0	10.0	0.08	40.0%
[25]	18.7 × 5.5	3.3–4.2	11	0.02	N/A
Pro	14.0 × 6.0	3.09–5.5	25.0	0.08	56.1%

※AAE = antenna array element. BW = bandwidth. ECC = envelope correlation coefficient. TE = total efficiency.

main direction of expression is the back and outside of the phone, which can greatly reduce interference during device use and is highly practical.

4. Component Comparison and Discussion

To verify the advantages and performance of the presented MIMO antenna, Table 1 compares the presented MIMO antenna with the most advanced technology in this field. The presented eight-element array antenna can be shown to have a relatively wide operating bandwidth (less than −6 dB), which provides excellent coverage of the 5G nR bands (*n*77/*n*78/*n*79) and the LTE 42 band with good isolation. The dimensions of the proposed antenna are also relatively small, and the efficiency and ECC of the antenna are comparable to those in the references. Therefore, the proposed 8-element array antenna has a relatively strong advantage.

5. Conclusion

For the application of 5G mobile devices, this paper proposes an isolation enhanced 8-unit MIMO antenna. The bandwidth of the antenna at −6 dB is 3.0–5.3 GHz, which covers the 5G nR bands (*n*76/*n*77/*n*78) and LTE42 bands. The measured bandwidth is 56.1%. The addition of the decoupling unit improves the isolation by 9 dB under simulated conditions and by 15 dB under actual measurements, reaching 25 dB. Additionally, the antenna also exhibits excellent ECC and radiation efficiency in the 5G nR frequency band. Compared with other 5G nR antennas, the antenna is also smaller in size. Therefore, the proposed 8-element MIMO antenna will be one of the favorable prospects for 5G terminal applications.

Data Availability

The data used to support the findings of this study are included within the article.

Conflicts of Interest

The authors declare that they have no conflicts of interest.

Acknowledgments

This research was funded in part by the National Natural Science Foundation of China, under Grant 62261052; in part by the Xinjiang Uygur Autonomous Region Natural Science Foundation General Project, under Grant 2022D01C424; in part by the Tianchi Talent Project in Xinjiang Uygur Autonomous Region, under Grant 510523005137; the Xinjiang University, under Grant 620321063; and in part by the China Postdoctoral Science Foundation, under grant 2022M722962.

References

[1] M. Agiwal, H. Kwon, and S. Park, "A survey on 4G-5G dual connectivity: road to 5G implementation," *IEEE Access*, vol. 9, pp. 16193–16210, 2021.

[2] P. Suthar, V. Agarwal, and R. S. Shetty, "Migration and interworking between 4g and 5g," in *Proceedings of the 2020 IEEE 3rd 5G World Forum (5GWF)*, pp. 401–406, Bangalore, India, September, 2020.

[3] D. Kim, *Road to 5G: Introduction and Migration*, GSM Association, London, U.K, 2018.

[4] E. G. Larsson, O. Edfors, F. Tufvesson, and T. L. Marzetta, "Massive MIMO for next generation wireless systems," *IEEE Communications Magazine*, vol. 52, no. 2, pp. 186–195, February 2014.

[5] L. Lu, G. Li, A. Swindlehurst, A. Ashikhmin, and R. Zhang, "An overview of massive MIMO: benefits and challenges," *IEEE Journal of Selected Topics in Signal Processing*, vol. 8, no. 5, pp. 742–758, Oct. 2014.

[6] K. Wong, J. Lu, L. Chen, W. Y. Li, and Y. L. Ban, "8-antenna and 16-antenna arrays using the quad-antenna linear array as a building block for the 3.5-GHz LTE MIMO operation in the smartphone," *Microwave and Optical Technology Letters*, vol. 58, no. 1, pp. 174–181, Jan. 2016.

[7] Z. Xu and C. Deng, "High-isolated MIMO antenna design based on pattern diversity for 5G mobile terminals," *IEEE Antennas and Wireless Propagation Letters*, vol. 19, no. 3, pp. 467–471, Mar. 2020.

[8] Y. Ye, X. Zhao, and J. Wang, "Compact high-isolated MIMO antenna module with chip capacitive decoupler for 5G mobile terminals," *IEEE Antennas and Wireless Propagation Letters*, vol. 21, no. 5, pp. 928–932, Mar. 2022.

[9] X. Zhao, S. Yeo, and L. Ong, "Decoupling of inverted-F antennas with high-order modes of ground plane for 5G mobile MIMO platform," *IEEE Transactions on Antennas and Propagation*, vol. 66, no. 9, pp. 4485–4495, Sep, 2018.

[10] C. Sim, H. Liu, and C. Huang, "Wideband MIMO antenna array design for future mobile devices operating in the 5G NR frequency bands n77/n78/n79 and LTE band 46," *IEEE Antennas and Wireless Propagation Letters*, vol. 19, no. 1, pp. 74–78, Jan. 2020.

[11] B. Yang, Y. Xu, J. Tong, Y. Zhang, Y. Feng, and Y. Hu, "Triport antenna with shared radiator and self-decoupling characteristic for 5G smartphone application," *IEEE Transactions on Antennas and Propagation*, vol. 70, no. 6, pp. 4836–4841, June 2022.

[12] L. Zhao, L. K. Yeung, and K. L. Wu, "A coupled resonator decoupling network for two-element compact antenna arrays in mobile terminals," *IEEE Transactions on Antennas and Propagation*, vol. 62, no. 5, pp. 2767–2776, May 2014.

[13] C. Wu, C. Chiu, and T. Ma, "Very compact fully lumped decoupling network for a coupled two-element array," *IEEE Antennas and Wireless Propagation Letters*, vol. 15, pp. 158–161, 2016.

[14] H. Piao, Y. Jin, Y. Xu, and L. Qu, "MIMO ground-radiation antennas using a novel closed-decoupling-loop for 5G applications," *IEEE Access*, vol. 8, pp. 142714–142724, 2020.

[15] L. Cui, J. Guo, Y. Liu, and C. Y. D. Sim, "An 8An 8-Element Dual-Band MIMO Antenna with Decoupling Stub for 5G Smartphone Applicationselement dual-band MIMO antenna with decoupling stub for 5G smartphone applications," *IEEE Antennas and Wireless Propagation Letters*, vol. 18, no. 10, pp. 2095–2099, 2019.

[16] A. Zhao and Z. Ren, "Multiple-input and multiple-output antenna system with self-isolated antenna element for fifth-generation mobile terminals," *Microwave and Optical Technology Letters*, vol. 61, no. 1, pp. 20–27, 2019.

[17] A. Zhao and Z. Ren, "Size reduction of self-isolated MIMO antenna system for 5G mobile phone applications," *IEEE Antennas and Wireless Propagation Letters*, vol. 18, no. 1, pp. 152–156, 2019.

[18] J. Kulkarni, J. Chen, and T. Zhang, "A broadband 8-antenna array design for 5G MIMO smartphone applications," in *Proceedings of the 2021 International Symposium on Antennas and Propagation (ISAP)*, pp. 1-2, Taipei, Taiwan, August, 2021.

[19] L. Chang, Y. Yu, K. Wei, and H. Wang, "Orthogonally-polarized dual antenna pair with high isolation and balanced high performance for 5G MIMO smartphone," *IEEE Transactions on Antennas and Propagation*, vol. 68, no. 5, pp. 3487–3495, May 2020.

[20] L. Sun, Y. Li, Z. Zhang, Z. Feng, and Z. Feng, "Wideband 5G MIMO antenna with integrated orthogonal-mode dual-antenna pairs for metal-rimmed smart-phones," *IEEE Transactions on Antennas and Propagation*, vol. 68, no. 4, pp. 2494–2503, 2020.

[21] W. Jiang, B. Liu, Y. Cui, and W. Hu, "High-isolation eight-element MIMO array for 5G smartphone applications," *IEEE Access*, vol. 7, pp. 34104–34112, 2019.

[22] X. Yuan, Z. Chen, T. Gu, and T. Yuan, "A wideband PIFA-pair-based MIMO antenna for 5G smartphones," *IEEE Antennas and Wireless Propagation Letters*, vol. 20, no. 3, pp. 371–375, 2021.

[23] J. Zhu, S. Li, and B. Feng, "Compact dual-polarized UWB quasi-self-complementary MIMO/diversity antenna with band-rejection capability," *IEEE Antennas and Wireless Propagation Letters*, vol. 15, pp. 905–908, 2016.

[24] J. Guo, L. Cui, and C. Li, "Side-edge frame printed eight-port dual-band antenna array for 5G smartphone applications," *IEEE Transactions on Antennas and Propagation*, vol. 66, no. 12, pp. 7412–7417, Dec, 2018.

[25] C. Sim, H. Chen, and J. Kulkarni, "Recent designs to achieving wideband MIMO antenna for 5G NR sub-6GHz smartphone applications," in *Proceedings of the 2020 International Symposium on Antennas and Propagation (ISAP)*, pp. 417-418, Osaka, Japan, March, 2021.